

Study on Stress-Temperature Coupled Damage Model of Warm Frozen Soil

Wei Shan¹, Tao Yang¹, Ying Guo¹, and Chengcheng Zhang¹

¹Northeast Forestry University

November 24, 2022

Abstract

Warm frozen soil is very sensitive to temperature change in the near phase transition region, and the relationship between temperature and physical and mechanical properties can be expressed by constitutive model. Based on the strain equivalent theory of damage mechanics, the damage model of warm frozen soil structure under the coupling action of stress and temperature is established. Based on Mohr-Coulomb criterion, the nominal stress is used to represent the stress damage of frozen soil element, the initial elastic modulus is used to represent the temperature damage, and the composite damage factor is introduced to describe the coupling relationship between them. Two methods are used to obtain the shape parameters and scale parameters of the coupled damage model: method 1 is the full fitting method based on the experimental data; method 2 is the semi-theoretical semi fitting method based on the characteristic points of the stress-strain curve. Through the triaxial compression test of frozen sand, it is proved that the simulation results of the stress-temperature coupled damage model are in good agreement with the experimental curves. Based on the experimental results, the results of the two methods are compared, and it is proved that method 2 is better than method 1 under the condition of strain softening. By comparing the predicted results of stress temperature coupled damage model and single stress damage model, it is shown that the former can effectively reduce the influence of parameter estimation error on the results and improve the stability of the model.

1 **Study on Stress-Temperature Coupled Damage Model of Warm Frozen Soil**

2 **Wei Shan, Tao Yang , Ying Guo, Chengcheng Zhang**

3 Cold region science and engineering institute, Northeast Forestry University, China.

4 Corresponding author: Wei Shan (shanwei456@163.com)

5 **Key Points:**

- 6
- The model can effectively predict the stress-strain relationship of warm frozen soil under the coupling effect of stress and temperature.
 - When strain softening, the shape and scale parameters are better solved according to the characteristic points of stress-strain curve.
 - Compared with the single stress damage model, the model can effectively reduce the influence of parameter estimation error on the results.
- 7
- 8
- 9
- 10
- 11

12

13

14 **Abstract**

15 Warm frozen soil is very sensitive to temperature change in the near phase transition region, and
16 the relationship between temperature and physical and mechanical properties can be expressed
17 by constitutive model. Based on the strain equivalent theory of damage mechanics, the damage
18 model of warm frozen soil structure under the coupling action of stress and temperature is
19 established. Based on Mohr- Coulomb criterion, the nominal stress is used to represent the stress
20 damage of frozen soil element, the initial elastic modulus is used to represent the temperature
21 damage, and the composite damage factor is introduced to describe the coupling relationship
22 between them. Two methods are used to obtain the shape parameters and scale parameters of the
23 coupled damage model: method 1 is the full fitting method based on the experimental data;
24 method 2 is the semi theoretical semi fitting method based on the characteristic points of the
25 stress-strain curve. Through the triaxial compression test of frozen sand, it is proved that the
26 simulation results of the stress-temperature coupled damage model are in good agreement with
27 the experimental curves. Based on the experimental results, the results of the two methods are
28 compared, and it is proved that method 2 is better than method 1 under the condition of strain
29 softening. By comparing the predicted results of stress temperature coupled damage model and
30 single stress damage model, it is shown that the former can effectively reduce the influence of
31 parameter estimation error on the results and improve the stability of the model.

32

33 **1 Introduction**

34 With the global warming and the rise of ground temperature, permafrost gradually
35 degenerates and the warm frozen soil stock further increases(Wei et al., 2011; Zhou et al.,
36 2000) .There is a close dynamic equilibrium relationship between the unfrozen water content and
37 the temperature. As a cemented phase, ice has a crucial influence on the mechanical properties of
38 frozen soil. The unfrozen water is very sensitive to the change of temperature in the near phase
39 transition region of warm frozen soil. Small temperature difference will directly lead to the
40 change of unfrozen water membrane thickness of frozen soil particles. The difference is reflected
41 in the mechanical index of frozen soil element and will be enlarged to a certain extent(Jin et al.,
42 2019; Xu, XZ et al., 2001; Yan et al., 2019). Compared with normal frozen soil, warm frozen
43 soil is essentially similar to the mixed state of thawed soil and frozen soil(Liu, S&Zhang, 2012).
44 This kind of material form makes the internal defects of permafrost unit more significant than
45 that of normal permafrost in terms of both the relative quantity and the influence on the
46 mechanical properties of soil(Lai et al., 2008; Li, S et al., 2009; Ning&Zhu, 2007). Due to the
47 high instantaneous strength of frozen soil, the elastic modulus of frozen soil is assumed to be a
48 certain value in numerical calculation(Liu, Z&Yu, 2011; Na&Sun, 2017; Zhang, M et al., 2017;
49 Zhang, Y&Michalowski, 2015). But for warm frozen soil, because of the increase of unfrozen
50 water content caused by the increase of temperature, the deterioration of frozen soil stiffness will
51 be more obvious(Jia et al., 2019). In the variable temperature environment, if the mechanical
52 parameters under a certain temperature fixed value are used for the numerical analysis of the
53 stress-strain relationship of frozen soil, it is easy to have problems such as the calculation result
54 error is too large, which will affect the safety of the facilities(Li, G, 2009).

55 The mechanical research of warm frozen soil mainly focuses on its strength
 56 characteristics, deformation characteristics and constitutive model, but the overall research of
 57 constitutive model is less(Liu, S&Zhang, 2012). Lai Yuanming et al. (Lai et al., 2008; Li, S et al.,
 58 2007)Showed that the distribution of strength and elastic modulus of warm frozen soil is discrete.
 59 The distribution of strength and elastic modulus of frozen soil can be described by Weibull
 60 distribution. Strain is taken as damage token and statistical damage mechanics is introduced to
 61 form the earliest damage model of warm frozen soil. According to Li Shuangyang et al. (Li, S et
 62 al., 2009), the concept of mechanical damage represented by strain is not clear enough and lacks
 63 theoretical support. Therefore, Mohr-Coulomb criterion is introduced to judge the damage state
 64 of warm frozen soil element, and the parameter expression in one-dimensional state is derived,
 65 which has achieved good results. The constitutive study of warm frozen soil has always focused
 66 on the deformation development under the action of single stress factor, and temperature is only
 67 a fixed condition rather than an action factor, which limits the application scope of the
 68 constitutive model to a certain extent(Lai et al., 2009; Zhang, D et al., 2018). At present, the
 69 research on the coupling effect of stress and temperature is mainly focused on the level of
 70 physical field control equation, while the research on the deeper constitutive model is less
 71 (Dumais & Konrad, 2017; Zhang, Y&Michalowski, 2015). According to the strain equivalent
 72 theory of damage mechanics, Zhang Huimei et al. (Zhang, H&Yang, 2010) obtained the
 73 composite damage model of freeze-thaw rock under the action of temperature and stress. Yu
 74 Songtao et al.(Yu et al., 2018)introduced H-B criterion to extend the application scope of the
 75 model to describe the stress-strain relationship of rock under the action of warm and confining
 76 pressure.

77 In view of the above problems and shortcomings, this paper introduces the composite
 78 damage theory into the stress-strain simulation prediction of warm frozen soil, establishes the
 79 stress-temperature coupling damage model characterized by Mohr-Coulomb criterion for the
 80 three-dimensional stress damage state of warm frozen soil element, and verifies the prediction
 81 effect of the model through relevant experiments, and discusses its effectiveness and stability.

82 **2 Stress-temperature coupled damage model**

83 Under the combined action of stress and temperature, the internal initial state of warm
 84 frozen soil will be damaged, some of the existing damage defects will further develop, and new
 85 damage defects will gradually form (Lai et al., 2008; Li, S et al., 2009). According to the damage
 86 theory of continuous medium, with the external action, the development of this kind of damage
 87 will show the decrease of the actual stress element in the stress body, which can be understood as
 88 the damage of material structure(Lemaitre, 2012). It is reflected in the physical parameters of the
 89 material, which is the reduction of the original material parameters, described by the damage
 90 factor. Under the action of nominal stress, the nominal strain due to material degradation is as
 91 follows:

$$92 \quad \varepsilon = \frac{\sigma}{\tilde{E}} = \frac{\sigma}{(1-D) \cdot E} \quad (1)$$

93 Where: σ is the nominal stress, ε is the nominal strain, E is the effective elastic modulus,
 94 \tilde{E} is the initial state of the elastic modulus.

95 2.1 Stress damage

96 Under the action of simple stress, the damage factor D_m can be expressed by the ratio of
 97 the number of damage elements $N(t)$ at a certain time to the number of damage elements N at the
 98 final failure:

$$99 \quad D_m = \frac{N(t)}{N} \quad (2)$$

100 A large number of experiments show that $N(t)$ obeys Weibull distribution(Lai et al.,
 101 2008). Its probability density function is:

$$102 \quad f(x) = \frac{m}{a} \cdot \left(\frac{x}{a}\right)^{m-1} \cdot \exp\left[-\left(\frac{x}{a}\right)^m\right] \quad (3)$$

103 Where m and a are the shape parameters and scale parameters of the distribution
 104 respectively.

105 So the expression of $N(t)$ is:

$$106 \quad \begin{aligned} N(t) &= \int_0^F N \cdot f(x) dx \\ &= N \cdot \left\{ 1 - \exp\left[-\left(\frac{F}{a}\right)^m\right] \right\} \end{aligned} \quad (4)$$

107 Therefore:

$$108 \quad D_m = \frac{N(t)}{N} = 1 - \exp\left[-\left(\frac{F}{a}\right)^m\right] \quad (5)$$

109 Among them, for the characterization of the number of unit damage F , Mohr-Coulomb
 110 theoretical analysis is used to determine(Li, S et al., 2009).

111 In triaxial compression test, Mohr-Coulomb shear strength formula can be expressed as
 112 follows by axial stress σ_1 and confining pressure σ_3 :

$$113 \quad \frac{1}{2} \cdot (\sigma_1 - \sigma_3) = c \cdot \cos \varphi - \frac{1}{2} \cdot (\sigma_1 + \sigma_3) \cdot \sin \varphi \quad (6)$$

114 If the terms σ_1 and σ_3 in the above formula are transferred, we can get:

$$115 \quad F = 2c \cdot \cos \varphi = (1 + \sin \varphi) \cdot \tilde{\sigma}_1 - (1 - \sin \varphi) \cdot \tilde{\sigma}_3 \quad (7)$$

116 Among them, σ_1 and σ_3 are the real stress of the material with the development of warm
 117 frozen soil damage. From the generalization of Formula 1, we can get:

$$118 \quad \varepsilon = \frac{\sigma}{(1 - D_m) \cdot E} = \frac{\tilde{\sigma}}{E} \quad (8)$$

119 Thus, the damage characterization quantity expressed by nominal stress F can be
120 established

$$121 \quad F = \left[(1 + \sin \varphi) \cdot \sigma_1 - (1 - \sin \varphi) \cdot \sigma_3 \right] / (1 - D_m) \quad (9)$$

122 According to the stress-strain relationship of materials under the action of three-
123 dimensional stress, it can be concluded that:

$$124 \quad \begin{aligned} \varepsilon_1 &= \frac{1}{E} \cdot \left[\sigma_1 - \nu \cdot (\sigma_2 + \sigma_3) \right] \\ &= \frac{1}{E \cdot (1 - D_m)} \cdot \left[\sigma_1 - \nu \cdot (\sigma_2 + \sigma_3) \right] \end{aligned} \quad (10)$$

125 In the triaxial compression experiment, $\sigma_2 = \sigma_3$, the expression of $1 - D_m$ can be obtained
126 by taking the above formula:

$$127 \quad 1 - D_m = (\sigma_1 - 2\nu \cdot \sigma_3) / E \cdot \varepsilon_1 \quad (11)$$

128 Take equation (11) into equation (9) to get:

$$129 \quad F = E \cdot \varepsilon_1 \cdot \left[(1 + \sin \varphi) \cdot \sigma_1 - (1 - \sin \varphi) \cdot \sigma_3 \right] / (\sigma_1 - 2\nu \cdot \sigma_3) \quad (12)$$

130 When the damage characterization F corresponding to different axial strain ε_1 is
131 calculated from the above formula, σ_1 in the formula is the unknown quantity to be solved.

132 It is assumed that in a small strain range, the damage evolution amount of frozen soil
133 element is small, and when reflected on the damage characterization amount F , the increment in
134 the small range can be ignored, so it can be expressed as follows:

$$135 \quad F_n = \begin{cases} E \cdot \varepsilon_{1_n} \cdot \left[(1 + \sin \varphi) \cdot \sigma_{1_{n-1}} - (1 - \sin \varphi) \cdot \sigma_{3_{n-1}} \right] / (\sigma_{1_{n-1}} - 2\nu \cdot \sigma_{3_{n-1}}) & n = 1 \\ E \cdot \varepsilon_{1_{n-1}} \cdot \left[(1 + \sin \varphi) \cdot \sigma_{1_{n-1}} - (1 - \sin \varphi) \cdot \sigma_{3_{n-1}} \right] / (\sigma_{1_{n-1}} - 2\nu \cdot \sigma_{3_{n-1}}) & n \geq 2 \end{cases} \quad (13)$$

136 Where the lower right corner mark n represents the accumulated step number of strain ε
137 when it is accumulated from $\varepsilon = 0$ in a certain step. When $n - 1 = 0$, it is the stress value
138 corresponding to the initial state before the bias load starts after the end of the confining pressure
139 load. At this time, $\sigma_1 = \sigma_3$, the above formula can be converted into the following form:

$$140 \quad F_n = \begin{cases} 2E \cdot \varepsilon_{1_n} \cdot \sin \varphi / (1 - 2\nu) & n = 1 \\ E \cdot \varepsilon_{1_{n-1}} \cdot \left[(1 + \sin \varphi) \cdot \sigma_{1_{n-1}} - (1 - \sin \varphi) \cdot \sigma_{3_{n-1}} \right] / (\sigma_{1_{n-1}} - 2\nu \cdot \sigma_{3_{n-1}}) & n \geq 2 \end{cases} \quad (14)$$

141 2.2 Temperature damage

142 The cementation force of ice on soil particles and its own strength in frozen soil provide
143 rigidity higher than that in melting state (Ning&Zhu, 2007). With the change of temperature, the
144 strength of ice decreases and the cementation ability decreases. This kind of composite material
145 degradation due to the effect of temperature can also be reflected by the concept of damage.

146 It can be seen from Formula 1 that the effect of material damage on mechanical
 147 parameters is most directly reflected in the reduction of elastic modulus.

148 Therefore, the temperature damage factor D_T is defined, which represents the
 149 deterioration degree of the initial state caused by the increase of temperature and the decrease of
 150 ice strength and cementation force in the frozen soil:

$$151 \quad D_T = 1 - \frac{E_T}{E} \quad (15)$$

152 Where E is the elastic modulus of warm frozen soil in the initial state, and E_T is the elastic
 153 modulus of a certain temperature after heating up. The relationship between the elastic modulus
 154 of frozen soil and temperature can be expressed by the following formula (Zhang, M et al., 2017):

$$155 \quad E_T = \beta + \gamma \cdot |T|^{0.6} \quad (16)$$

156 β and γ are the experimental parameters.

157 2.3 Coupling effect of stress and temperature

158 According to the theory of strain equivalence, the composite damage caused by
 159 temperature and stress can be deduced. It can be characterized by composite damage factors D_c
 160 (Zhang, H&Yang, 2010):

$$161 \quad D_c = D_m + D_T - D_m \cdot D_T \quad (17)$$

162 Take formula (5) and formula (15) into formula (17) to get:

$$163 \quad D_c = 1 - \frac{E_T}{E} \cdot \exp \left[-\left(\frac{F}{a}\right)^m \right] \quad (18)$$

164 Take equation (16) into equation (18) and simplify it to obtain:

$$165 \quad D_c = 1 - \frac{1 + \lambda \cdot |T|^{0.6}}{1 + \lambda \cdot |T_0|^{0.6}} \cdot \exp \left[-\left(\frac{F}{a}\right)^m \right] \quad (19)$$

166 Where T_0 is the temperature of the initial state and λ is defined as the temperature
 167 deterioration coefficient:

$$168 \quad \lambda = \frac{\gamma}{\beta} \quad (20)$$

169 Equation (19) is introduced into equation (1), which is the stress-temperature coupled
 170 damage model of worm frozen soil:

$$171 \quad \varepsilon_1 = \frac{(\sigma_1 - 2\nu \cdot \sigma_3) \cdot [1 + \lambda \cdot |T_0|^{0.6}]}{[1 + \lambda \cdot |T|^{0.6}] \cdot \exp \left[-\left(\frac{F}{a}\right)^m \right]} \cdot E \quad (21)$$

172 3 Model parameter

173 The stress damage of warm frozen soil accords with the Weibull distribution(Li, S et al.,
174 2007). The shape parameter m and scale parameter a in this distribution are two important
175 parameters in the stress-temperature coupling model. Their values are directly affected by the
176 stress-strain curve. Due to the different confining pressure and soil properties, the curves of
177 deviator stress $\sigma_1 - \sigma_3$ and axial strain ε_1 obtained from triaxial test of warm frozen soil will take
178 different forms(Li, G, 2009; Song et al., 2019).

179 In general, the stress-strain curves of frozen sand, frozen silty sand and frozen silty clay
180 with high moisture content will show strain softening type, and the partial stress has a peak
181 value. After the peak strain, the partial stress decreases with the increase of strain(Esmaeili-Falak
182 et al., 2017; Qi&MA, 2010; Xu, Xiangtian et al., 2016). For the fine-grained soil with low water
183 content, the stress-strain curve has no obvious peak value, and the partial stress gradually
184 increases with the increase of axial strain, but the growth rate gradually decreases, and finally
185 tends to be stable(Ma et al., 1999).

186 For two different stress-strain curves, there are two typical two parameter solutions of
187 Weibull distribution.

188 One is to get the values of shape parameters m and scale parameters a by linear fitting
189 (method 1).The other is to further deduce formula (12) through the data of characteristic points in
190 the stress-strain curve, and obtain the expression of shape parameters m and scale parameters a
191 expressed by the numerical value of characteristic points (method 2) (Cao&Zhang, 2005; Xu,
192 W&Wei, 2002).

193 Method 1: this method can be applied to both strain hardening and strain softening stress-
194 strain curves.

195 Joint formula (5) and (11)

$$196 \exp \left[- \left(\frac{F}{a} \right)^m \right] = (\sigma_1 - 2\nu \cdot \sigma_3) / E \cdot \varepsilon_1 \quad (22)$$

197 The following formula can be obtained by two logarithm operations at both ends of the
198 equation:

$$199 \ln \left\{ - \ln \left[(\sigma_1 - 2\nu \cdot \sigma_3) / E \cdot \varepsilon_1 \right] \right\} = m \ln F - m \ln a \quad (23)$$

200 Among them, the left-hand items and the right-hand F of the equation can be obtained
201 through the triaxial experiment. Therefore order:

$$202 Y = \ln \left\{ - \ln \left[(\sigma_1 - 2\nu \cdot \sigma_3) / E \cdot \varepsilon_1 \right] \right\} \quad (24)$$

$$203 X = \ln F \quad (25)$$

$$204 C = -m \ln a \quad (26)$$

205 Then we can get the linear relationship of the three:

$$206 Y = mX + C \quad (27)$$

207 A set of X and Y values corresponding to the experimental curve under a certain
 208 confining pressure and temperature can be obtained by introducing the triaxial experimental
 209 values. The expression of the final shape parameters m and scale parameters a can be obtained by
 210 linear fitting and further calculation:

$$211 \quad m = \frac{Y - C}{X} \quad (28)$$

$$212 \quad a = \exp\left(-\frac{C}{m}\right) \quad (29)$$

213 The detailed calculation method of relevant parameters will be further explained in the
 214 later experimental verification part.

215 Method 2: this method is only suitable for strain softening.

216 First, deform equation (22) to obtain:

$$217 \quad \begin{aligned} \sigma_1 &= \tilde{E} \cdot \varepsilon_1 + 2\nu \cdot \sigma_3 \\ &= E \cdot \varepsilon_1 \cdot \exp\left[-\left(\frac{F}{a}\right)^m\right] + 2\nu \cdot \sigma_3 \end{aligned} \quad (30)$$

218 According to the generalized Hooke's law, the relationship between ε_3 and axial stress σ_1 ,
 219 confining pressure σ_3 can be established.

$$220 \quad \begin{aligned} \varepsilon_3 &= \frac{1}{\tilde{E}} \cdot [\sigma_3 - \nu \cdot (\sigma_1 + \sigma_2)] \\ &= \frac{1}{E \cdot (1 - D_m)} \cdot [(1 - \nu) \cdot \sigma_3 - \nu \cdot \sigma_1] \end{aligned} \quad (31)$$

221 If the above formula is deformed and brought in (5), you can get:

$$222 \quad \begin{aligned} \sigma_3 &= (\tilde{E} \cdot \varepsilon_3 + \nu \cdot \sigma_1) / (1 - \nu) \\ &= \left(E \cdot \varepsilon_3 \cdot \exp\left[-\left(\frac{F}{a}\right)^m\right] + \nu \cdot \sigma_1 \right) / (1 - \nu) \end{aligned} \quad (32)$$

223 Taking the peak stress of strain softening curve as the characteristic point, the following
 224 relationship can be obtained:

$$225 \quad \begin{cases} \varepsilon_1 = \varepsilon_p \\ \sigma_1 = \sigma_p \end{cases} \quad (33)$$

$$226 \quad \begin{cases} \varepsilon_1 = \varepsilon_p \\ \frac{d\sigma_1}{d\varepsilon_1} = 0 \end{cases} \quad (34)$$

227 Find the total differential of formula (30) and formula (32), and the results are as follows:

$$d\sigma_1 = \frac{\partial \sigma_1}{\partial \varepsilon_1} d\varepsilon_1 + \frac{\partial \sigma_1}{\partial F} dF + \frac{\partial \sigma_1}{\partial a} da + \frac{\partial \sigma_1}{\partial m} dm + 2vd\sigma_3 \quad (35)$$

$$d\sigma_3 = \frac{\partial \sigma_3}{\partial \varepsilon_3} d\varepsilon_3 + \frac{\partial \sigma_3}{\partial F} dF + \frac{\partial \sigma_3}{\partial a} da + \frac{\partial \sigma_3}{\partial m} dm + \frac{v}{1-v} d\sigma_1 \quad (36)$$

The selected damage characterization quantity is determined based on Mohr-Coulomb theory. When equation (30) is brought into equation (7), the F expressed by ε_1 and σ_3 can be obtained. For the convenience of distinction, the F is marked as F^1 :

$$F^1 = (1 + \sin \varphi) \cdot (E \cdot \varepsilon_1 + 2v \cdot \sigma_3) - (1 - \sin \varphi) \cdot \sigma_3 \quad (37)$$

In the same way, if you take equation (32) into equation (7), you can get F represented by ε_3 and σ_3 , marked F^3 :

$$F^3 = (1 + \sin \varphi) \cdot \left(\frac{1-v}{v} \cdot \sigma_3 - \frac{E}{v} \cdot \varepsilon_3 \right) - (1 - \sin \varphi) \cdot \sigma_3 \quad (38)$$

Find the total differential of formula (37) and formula (38), and the results are as follows:

$$dF^1 = \frac{\partial F^1}{\partial \varepsilon_1} d\varepsilon_1 + \frac{\partial F^1}{\partial \sigma_3} d\sigma_3 \quad (39)$$

$$dF^3 = \frac{\partial F^3}{\partial \varepsilon_3} d\varepsilon_3 + \frac{\partial F^3}{\partial \sigma_3} d\sigma_3 \quad (40)$$

In the application of frozen soil damage model, the shape parameter m and the scale parameter a are often regarded as only related to the confining pressure σ_3 (Li, S et al., 2009; Zhang, D et al., 2018), so the following relationship can be obtained:

$$da = \frac{\partial a}{\partial \sigma_3} d\sigma_3 \quad (41)$$

$$dm = \frac{\partial m}{\partial \sigma_3} d\sigma_3 \quad (42)$$

If equation (39), (41) and (42) are introduced into equation (35), the total differential relations of σ_1 , σ_3 and ε_1 can be obtained:

$$d\sigma_1 = \left(\frac{\partial \sigma_1}{\partial \varepsilon_1} + \frac{\partial \sigma_1}{\partial F} \cdot \frac{\partial F^1}{\partial \varepsilon_1} \right) d\varepsilon_1 + Pd\sigma_3 \quad (43)$$

Upper form:

$$P = \frac{\partial \sigma_1}{\partial F} \cdot \frac{\partial F^1}{\partial \sigma_3} + \frac{\partial \sigma_1}{\partial a} \cdot \frac{\partial a}{\partial \sigma_3} + \frac{\partial \sigma_1}{\partial m} \cdot \frac{\partial m}{\partial \sigma_3} + 2v \quad (44)$$

If equation (40), (41) and (42) are introduced into equation (36), the total differential relations of σ_1 , σ_3 and ε_3 can be obtained:

$$252 \quad \frac{\nu}{\nu-1} d\sigma_1 = \left(\frac{\partial \sigma_3}{\partial \varepsilon_3} + \frac{\partial \sigma_3}{\partial F} \cdot \frac{\partial F^2}{\partial \varepsilon_3} \right) d\varepsilon_3 + Q d\sigma_3 \quad (45)$$

253 Upper form:

$$254 \quad Q = \frac{\partial \sigma_3}{\partial F} \cdot \frac{\partial F^2}{\partial \sigma_3} + \frac{\partial \sigma_3}{\partial a} \cdot \frac{\partial a}{\partial \sigma_3} + \frac{\partial \sigma_3}{\partial m} \cdot \frac{\partial m}{\partial \sigma_3} - 1 \quad (46)$$

255 The total differential relations of σ_1 , ε_1 and ε_3 can be obtained by combining equations
256 (43) and (45):

$$257 \quad d\sigma_1 = R d\varepsilon_1 + S d\varepsilon_3 \quad (47)$$

258 Upper form:

$$259 \quad R = \frac{\partial \sigma_1}{\partial \varepsilon_1} = \frac{(1-\nu) \cdot Q}{\nu \cdot P + Q \cdot (1+\nu)} \cdot \left(\frac{\partial \sigma_1}{\partial \varepsilon_1} + \frac{\partial \sigma_1}{\partial F} \cdot \frac{\partial F^1}{\partial \varepsilon_1} \right) \quad (48)$$

$$260 \quad S = \frac{\partial \sigma_1}{\partial \varepsilon_3} = \frac{(1-\nu) \cdot Q}{\nu \cdot P + Q \cdot (1+\nu)} \cdot \left(\frac{\partial \sigma_3}{\partial \varepsilon_3} + \frac{\partial \sigma_3}{\partial F} \cdot \frac{\partial F^2}{\partial \varepsilon_3} \right) \quad (49)$$

261 The numerical conditions of the characteristic points of the stress-strain curve are
262 introduced to solve the problem. First, formula (33) is introduced into formula (30) to obtain:

$$263 \quad \exp \left[- \left(\frac{F_p}{a} \right)^m \right] = \frac{\sigma_p - 2\nu \cdot \sigma_3}{E \cdot \varepsilon_p} \quad (50)$$

264 Upper form:

$$265 \quad F_p = (1 + \sin \varphi) \cdot (E \cdot \varepsilon_p + 2\nu \cdot \sigma_3) - (1 - \sin \varphi) \cdot \sigma_3 \quad (51)$$

266 Then formula (34) is introduced into formula (48) and simplified to obtain:

$$267 \quad \left. \frac{\partial \sigma_1}{\partial \varepsilon_1} \right|_{\varepsilon_1=\varepsilon_p} + \left. \frac{\partial \sigma_1}{\partial F} \cdot \frac{\partial F^1}{\partial \varepsilon_1} \right|_{\varepsilon_1=\varepsilon_p} = 0 \quad (52)$$

268 After each value is brought in, it can be simplified to obtain:

$$269 \quad \left(\frac{F_p}{a} \right)^m = \frac{F_p}{E \cdot \varepsilon_p \cdot (1 + \sin \varphi) \cdot m} \quad (53)$$

270 The expression of shape parameter m and scale parameter a can be obtained by combining
271 formula (50) and formula (53):

$$272 \quad m = F_p / \left[E \cdot \varepsilon_p \cdot (1 + \sin \varphi) \cdot \ln \frac{E \cdot \varepsilon_p}{\sigma_p - 2\nu \cdot \sigma_3} \right] \quad (54)$$

$$273 \quad a = F_p \cdot \left[\frac{E \cdot \varepsilon_p \cdot (1 + \sin \varphi) \cdot m}{F_p} \right]^{1/m} \quad (55)$$

274 The values in the above two formulas can be obtained from the curves of deviator stress
 275 and axial strain in triaxial compression experiments. If the confining pressure $\sigma_3 = 0$, formula
 276 (54) and formula (55) are reduced to one-dimensional uniaxial compression:

$$277 \quad m = 1 / \ln \frac{E \cdot \varepsilon_p}{\sigma_p} \quad (56)$$

$$278 \quad a = F_p \cdot (m)^{\frac{1}{m}} \quad (57)$$

279 Comparisons show that the results of uniaxial compression derived by predecessors are
 280 the same(Li, S et al., 2009).

281 4 Experimental verification

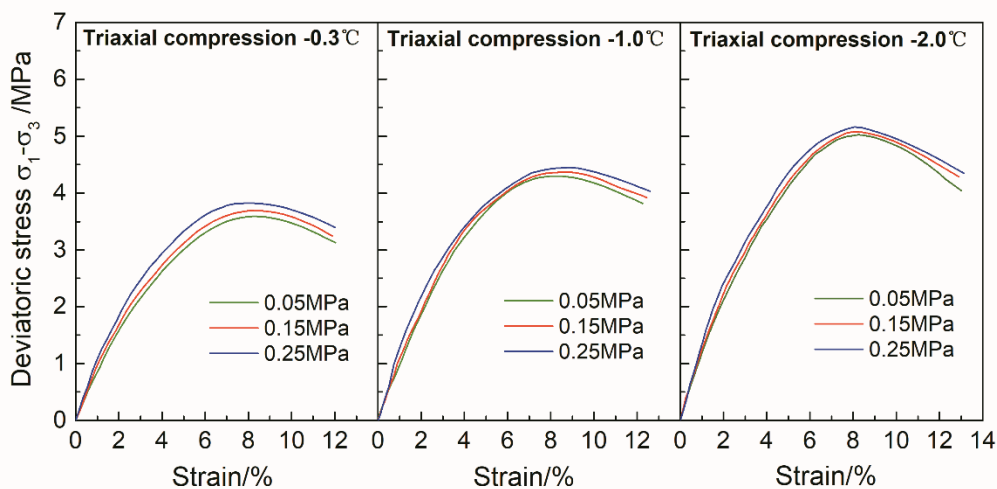
282 4.1 Determination of basic parameters

283 The model parameters are determined by temperature-controlled triaxial compression test
 284 of frozen sand. The composition of fine sand particles used is shown in Table 1.

285 **Table 1.** Particle Composition of Fine Sand for Experiment

Particle composition/%				
>0.5mm	0.5~0.25mm	0.25~0.10mm	0.10~0.075mm	<0.075mm
2.7	30.6	43.9	19.7	3.1

286 The specimens with diameter of 39.1mm, height of 80mm and dry weight of 15.3kN/m³
 287 after compaction preparation were saturated and frozen for 48h in a low temperature tank at -
 288 25°C. Three sets of triaxial compression experiments were carried out at a loading rate of 1
 289 mm/min and a temperature of -0.3°C, -1°C, and -2°C, respectively, at a constant temperature of
 290 24h in the target temperature chamber before the experiment. The confining pressures of each
 291 group were 50 kPa, 150 kPa and 250 kPa, respectively. The experimental results are shown in
 292 Figure. 1.



293

294

Figure 1. Triaxial compression test stress-strain curve of frozen sand

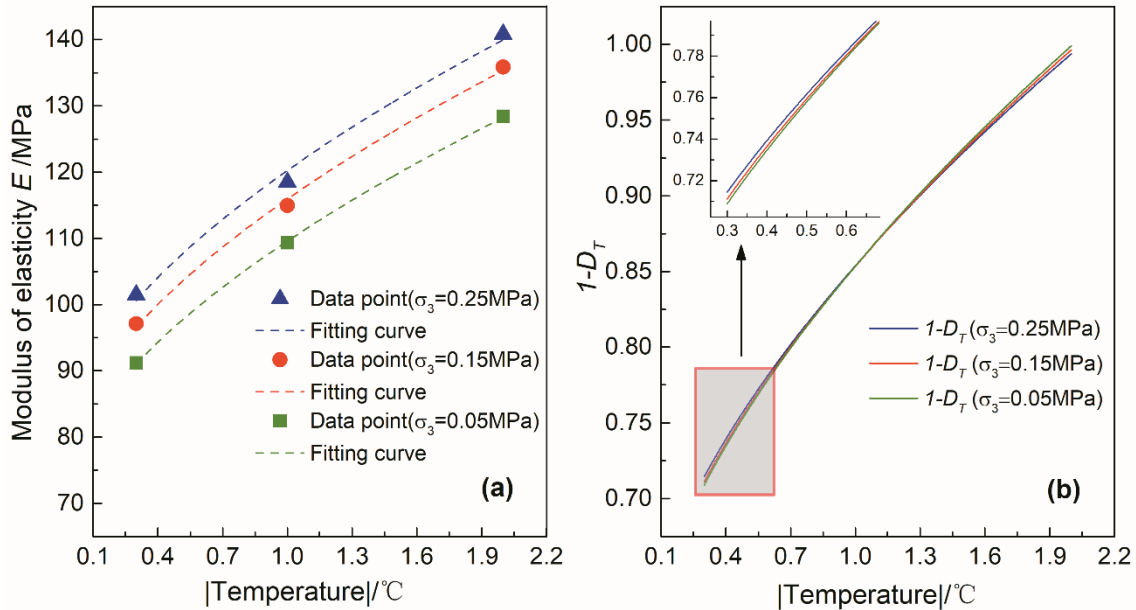
295 As can be seen from Figure. 1, the stress-strain curve approximates a linear change at the
 296 initial stage of strain. The elastic modulus of equation (15) characterizes the initial undamaged
 297 state of the frozen soil, and the closer the value is to the initial elastic modulus, the more precise
 298 the model solution is. Therefore, the modulus of the linear elastic section in the range of 0-0.5%
 299 strain is approximated as the elastic modulus E of the initial damage state. The basic mechanical
 300 parameters calculated from the experimental results are shown in Table 2.

301 **Table 2. Basic Mechanical Parameters of the Model**

Temperature/ $^{\circ}\text{C}$	-0.3			-1.0			-2.0		
Confining pressure/MPa	E/MPa	$\varphi/^{\circ}$	ν	E/MPa	$\varphi/^{\circ}$	ν	E/MPa	$\varphi/^{\circ}$	ν
0.05	91.16			109.33			128.39		
0.15	97.12	21.56	0.2623	114.95	15.85	0.2513	135.85	14.66	0.2452
0.25	101.51			118.51			140.84		

302 According to the data in Table 2, the expression of temperature damage modulus E_T in the
 303 stress temperature coupled damage model can be obtained from equation (16).

304 It can be seen from the above analysis that in theory, only the confining pressure is
 305 required to be controlled, and β and γ in equation (16) should be a pair of constants. The elastic
 306 modulus values corresponding to the three groups of confining pressures in Table 2 are fitted and
 307 calculated, and the temperature damage factor D_T corresponding to the fitting curve is compared.
 308 The results are shown in Figure. 2.



309 **Figure 2. Fitting curve of elastic modulus and corresponding damage factors under**
 310 **different confining pressures. (a) Fitting curve of initial modulus of elasticity with temperature**
 311 **under three confining pressures 0.05MPa, 0.15MPa and 0.25MPa. (b) Temperature damage**
 312 **factors corresponding to three confining pressure states 0.05MPa, 0.15MPa and 0.25MPa when -**
 313 **2 $^{\circ}\text{C}$ is taken as non-destructive state.**
 314

315 It can be seen from Figure. 2 (a) that although the fitting curves corresponding to the
 316 three groups of data are not the same, Figure. 2 (b) shows that the change curve of the final

317 damage factor is basically the same, so the fitting curve corresponding to the data with confining
 318 pressure of 0.05MPa is selected as the expression of elastic modulus E_T .

319
$$E_T = 73.47 + 36.14|T|^{0.6} \tag{58}$$

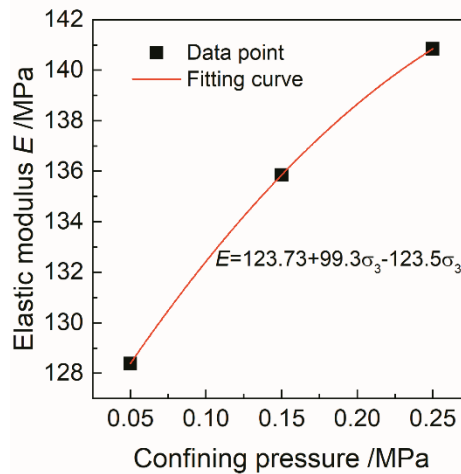
320 The goodness of fit $R^2 = 0.9998$, which can reflect the change of data more accurately.

321 It can be seen from table 2 that when the confining pressure changes, the elastic modulus
 322 will also change. In order to make the model more applicable, it is necessary to fit the
 323 relationship between elastic modulus and confining pressure at the same temperature.

324 In the verification experiment, the nondestructive temperature is $-2.0\text{ }^\circ\text{C}$ (Liu, S&Zhang,
 325 2012), and the relationship between elastic modulus and confining pressure is:

326
$$E = 123.73 + 99.3\sigma_3 - 123.5\sigma_3^2 \tag{59}$$

327 The fitting curve is shown in Figure. 3.



328 **Figure3.** Fitting curve of the relationship between elastic modulus and confining pressure
 329

330 4.2 Parameter determination of damage model

331 According to the data in Figure. 1, the shape parameter m and scale parameter a of the
 332 stress damage model are solved by the above two methods. The final settlement results are
 333 shown in Table 3 and Table 4. Among them, Table 3 is the full fitting formula of formula (12),
 334 (24), (25), (26) and (27) in method 1; Table 4 is the semi theoretical semi fitting formula of
 335 formula (51), (54) and (55) in method 2.

336 **Table 3.** Summary of Solution of Shape Parameter m and Scale Parameter a (Method 1)

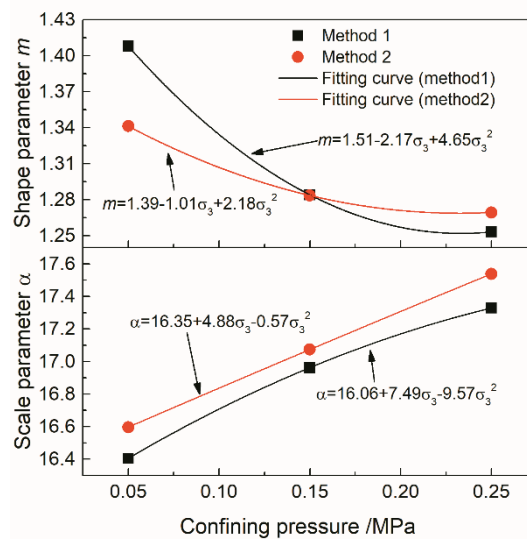
Temperature/ $^\circ\text{C}$	-0.3		-1.0		-2.0	
Confining pressure /MPa	m	a	m	a	m	a
0.05	1.3680	12.8596	1.3090	14.4286	1.4080	16.4050
0.15	1.3030	13.5591	1.2170	14.9914	1.2840	16.9624
0.25	1.2650	14.3200	1.1850	15.4883	1.2530	17.3285

338 **Table 4.** Summary of Solution of Shape Parameter m and Scale Parameter a (Method 2)

Temperature/°C	-0.3		-1.0		-2.0	
Confining pressure /MPa	m	a	m	a	m	a
0.05	1.3452	12.9657	1.3501	14.4209	1.3412	16.5967
0.15	1.3206	13.5783	1.2086	15.1146	1.2834	17.0735
0.25	1.3046	14.2468	1.1698	15.6325	1.2692	17.5389

339 In order to obtain the stress-strain curve under the condition of nonparametric
 340 experimental confining pressure, polynomial fitting is used to fit the relationship between the
 341 shape parameter m and scale parameter a with the confining pressure.

342 Fit the parameter value when the experimental temperature is -2°C , and the fitting curve
 343 is as shown in Figure. 4.



344 **Figure 4.** Fitting curve of shape parameter m and scale parameter a to the change of
 345 confining pressure
 346

347 The final fitting polynomial is shown in the following formula, where equation (60) is the
 348 parameter fitting equation obtained by method 1, and equation (61) is the parameter fitting
 349 equation obtained by method 2.

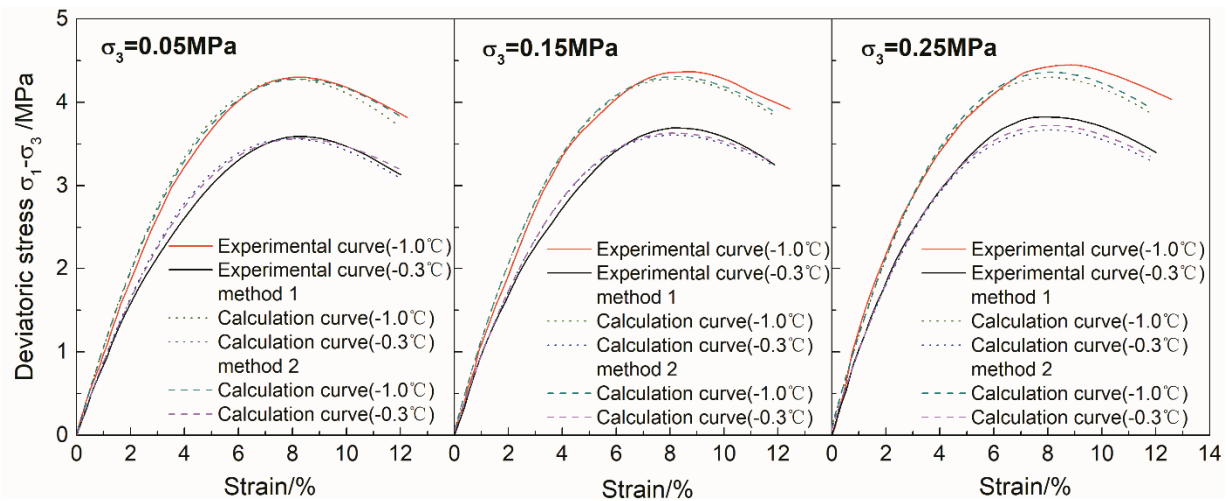
$$350 \quad \begin{cases} m = 1.51 - 2.17\sigma_3 + 4.65\sigma_3^2 \\ a = 16.06 + 7.49\sigma_3 - 9.57\sigma_3^2 \end{cases} \quad (60)$$

$$351 \quad \begin{cases} m = 1.39 - 1.01\sigma_3 + 2.18\sigma_3^2 \\ a = 16.35 + 4.88\sigma_3 - 0.57\sigma_3^2 \end{cases} \quad (61)$$

352 4.3 Verification of experimental results

353 According to the above constant temperature to determine the confining pressure triaxial
 354 compression test results and the parameters obtained from calculation and analysis, the model is
 355 verified. First of all, the non-destructive state of the temperature damage calculation is taken as -

356 2.0°C, and the stress-strain curves at -0.3°C and -1.0°C are reconstructed with the data
 357 parameters, and compared with the experimental curves.



358
 359 **Figure 5.** Comparison of the calculated values of -0.3°C and -1.0°C damage models when
 360 -2.0°C is the non-destructive temperature

361 It can be seen from Figure. 5 that the overall simulation results of the model are good,
 362 among which the model simulation results are the most accurate when the confining pressure is
 363 0.05MPa, and there is a certain deviation when the bias stress simulation is 0.25MPa. By
 364 comparing the simulation accuracy of the three groups of confining pressure curves to the
 365 original experimental curves, it can be found that with the increase of confining pressure, the
 366 deviation degree of the calculated curves from the experimental curves increases gradually. At
 367 the same time of confining pressure, the model is more accurate for the experimental simulation
 368 results with higher temperature.

369 The influence of the two methods on the simulation results is compared. As can be easily
 370 seen from Figure. 5, the simulation results of the parameters obtained by method 2 are closer to
 371 the experimental curve than those obtained by method 1. When the confining pressure is small,
 372 the difference between the two methods is not big, but with the increase of confining pressure,
 373 the difference between the calculation curve of method 2 and the experimental curve is obviously
 374 smaller than that of method 1. The above verification process shows that the simulation results of
 375 the stress temperature coupled damage model have a high accuracy under the condition that the
 376 stress damage amount and the temperature damage amount corresponding to the target
 377 temperature are known.

378 Furthermore, through the temperature controlled triaxial compression experiment, the
 379 simulation prediction ability of the model to the actual stress-strain curve is verified when the
 380 model parameters are predicted according to the fitting polynomials in the preset stress and
 381 temperature range.

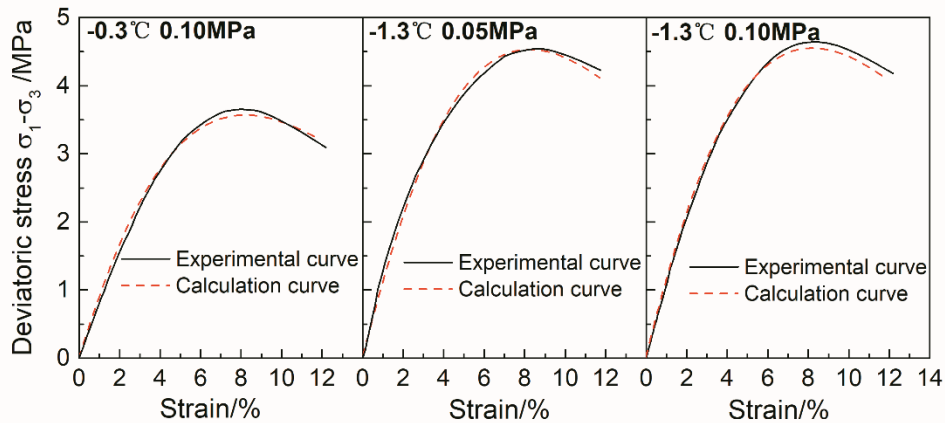
382 Three groups of experimental conditions were selected: ① the confining pressure was
 383 0.10MPa, and the experimental temperature was -0.3°C; ② the confining pressure was 0.05MPa,
 384 and the experimental temperature was -1.3°C; ③ the confining pressure was 0.10MPa, and the
 385 experimental temperature was -1.3°C. According to equations (58), (59) and (61), the parameters

386 required for the model calculation under the corresponding temperature and confining pressure
 387 are calculated, and the calculation results are shown in Table 5.

388 **Table 5.** Calculation Results of Damage Model Parameters Fitting Polynomials

Confining pressure /MPa	0.05				0.10			
Temperature/°C	E_T	E	m	a	E_T	E	m	a
-0.3	91.02				91.02			
-1.3	115.77	128.39	1.3450	16.5926	115.77	132.43	1.3108	16.8323

389 According to the parameters in Table 5, the final calculation curve is compared with the
 390 experimental curve as shown in Figure. 6.



391
 392 **Figure 6.** Comparison between experimental curve and calculation curve of temperature
 393 controlled triaxial compression test

394 It can be seen from Figure. 6 that the calculation curve obtained by using the damage
 395 model parameters can accurately simulate the stress growth with strain in the stress growth stage,
 396 while in the stress peak prediction, the simulation results under the condition of small confining
 397 pressure are still better than those under the condition of large confining pressure.

398 In the three groups of verification experiments shown in Figure. 6, the first two groups of
 399 experimental verification calculation respectively used the fitting values of the elastic modulus E
 400 corresponding to 0.10MPa at -2.0°C , the double parameters of Weibull distribution and the
 401 elastic modulus E_T representing temperature damage, while the third group used the fitting
 402 calculation formula for all the above four parameters. Compared with the simulation results, it is
 403 not difficult to find that there is a certain difference between the fitting value and the actual
 404 value, and the more the difference is introduced, the greater the impact on the results will be.
 405 Therefore, in the process of practical application, we should try to ensure that the experimental
 406 conditions of parameters are close to the actual working conditions, so as to improve the
 407 simulation accuracy.

408 5 Model discussion

409 As two important factors affecting the mechanical properties of frozen soil, confining
 410 pressure and temperature are a problem that must be faced in the practical application of damage
 411 model (Nassr et al., 2018; Xu, Xiangtian et al., 2019). In most cases, the experimental conditions

412 of parameters can not fully correspond to the actual conditions, so the fitting prediction of model
 413 parameters can not be avoided. It is easy to see from Table 2 and Table 4 that the elastic modulus
 414 E , shape parameter m and scale parameter a all change with the confining pressure and
 415 temperature. The stress-strain curve of frozen soil is predicted only by stress damage without
 416 considering the coupling damage of stress and temperature. Therefore, the parameter values
 417 corresponding to different confining pressures and temperatures are expressed by binary
 418 polynomials, and the parameters are predicted according to the polynomials.

419 The fitting polynomials are as follows.

$$420 \quad E = 79.76 + 27.63|T| + 76.24\sigma_3 - 2.63|T|^2 - 101.67\sigma_3^2 + 6.87|T| \cdot \sigma_3 \quad (62)$$

$$421 \quad a = 11.8974 + 2.2915|T| + 7.5042\sigma_3 - 0.0416|T|^2 - 2.1883\sigma_3^2 - 1.0208|T| \cdot \sigma_3 \quad (63)$$

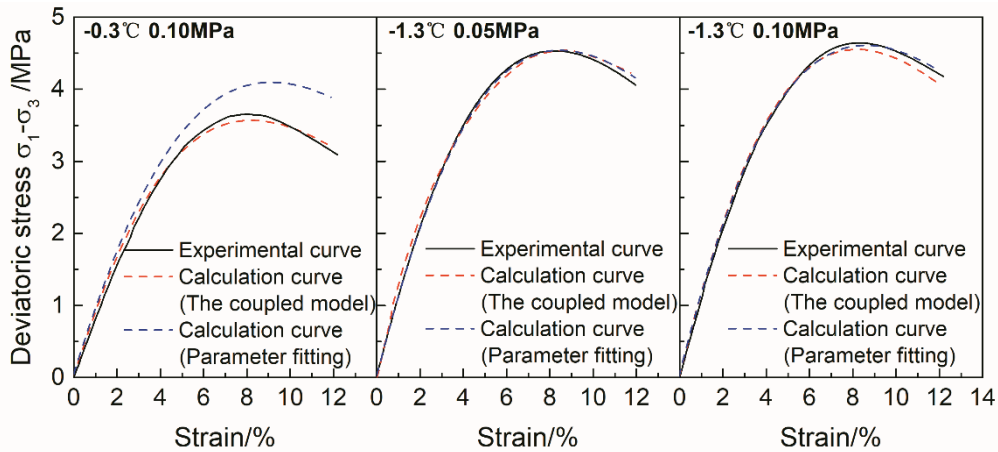
$$422 \quad m = 1.4941 - 0.2381|T| - 1.2088\sigma_3 + 0.1002|T|^2 + 2.5817\sigma_3^2 - 0.0489|T| \cdot \sigma_3 \quad (64)$$

423 At the same time, it can be seen from Table 2 that the friction angle and Poisson's ratio
 424 also change with the change of temperature, and the polynomial fitting method is still used for
 425 prediction.

$$426 \quad \varphi = 25.24 - 13.49|T| + 4.10|T|^2 \quad (65)$$

$$427 \quad \nu = 0.2687 - 0.0231|T| + 0.0057|T|^2 \quad (66)$$

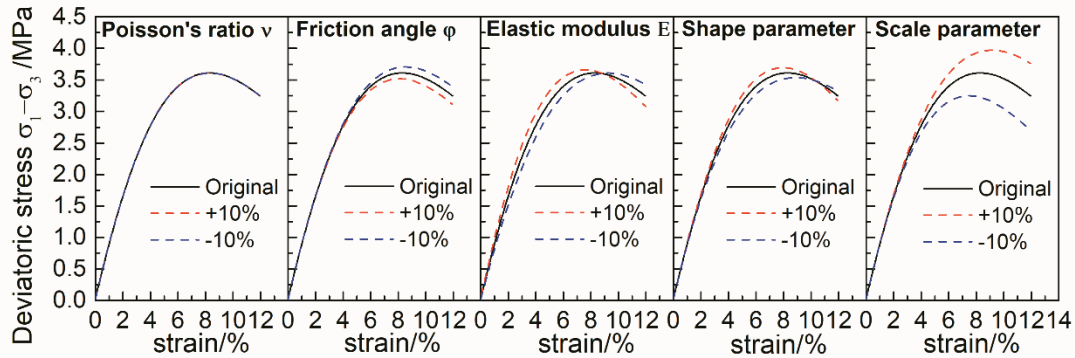
428 According to formula (58) - (66), calculate the experimental parameter data of
 429 temperature controlled triaxial compression described in the previous section, and compare the
 430 calculation results of stress temperature coupled damage model, as shown in Figure. 7.



431
 432 **Figure 7.** Comparison of results of stress-temperature coupled model and conventional
 433 parameter fitting

434 It can be seen from Figure. 7 that the simulation results of the latter two groups of
 435 experiments are more accurate only by parameter fitting. When the temperature is -1.3°C and the
 436 confining pressure is 0.10MPa, the simulation results are even better than the stress-temperature
 437 coupled damage model to some extent. However, the simulation results of the first group of
 438 experiments gradually deviate from the actual stress-strain curve in the stress growth stage, and
 439 the deviation of the final simulation results is too large.

440 Now the error sources of the above simulation methods are analyzed. Based on the
 441 calculation parameters of the damage model under the experimental temperature of -0.3°C and
 442 the experimental confining pressure of 0.05MPa , the influence of 10% increase or decrease of
 443 each parameter on the calculation curve is compared. The final result is shown in Figure. 8.



444

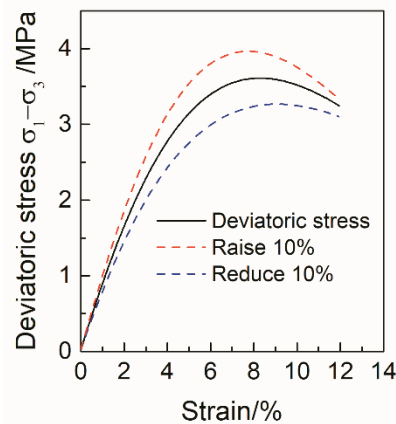
445 **Figure 8.** Comparison of the influence of 10% increase and 10% decrease of each
 446 parameter of the model on the calculation curve

447 When each parameter increases or decreases by 10% on the original datum parameter, the
 448 Poisson's ratio ν error has negligible effect on the final calculation curve compared with the
 449 original calculation curve. The influence of the error of friction angle φ and scale parameter a on
 450 the calculation results is mainly reflected in the peak value. With the increase of friction angle φ ,
 451 the peak strain decreases and the peak deviator stress decreases. On the contrary, with the
 452 increase of the scale parameter a , the peak deviator stress and strain increase simultaneously.
 453 The friction angle φ increases by 10%, the peak strain decreases by 2.41% and the peak deviator
 454 stress decreases by 2.55%. The friction angle φ decreases by 10%, the peak strain increases by
 455 2.41% and the peak deviator stress increases by 2.71%. When the scale parameter a increases or
 456 decreases by 10%, the peak strain increases or decreases by 10.25% compared with the reference
 457 value, and the peak deviator stress increases or decreases by 10.01%. It can be seen that the
 458 model results are more sensitive to the changes of scale parameters a .

459 The elastic modulus E and the shape parameter m have an effect on the stress growth, the
 460 peak value of stress and the stress decline stage of the calculation curve, and their overall change
 461 trends are the same. In the stress growth stage, the larger the parameter value is, the faster the
 462 stress growth is, and the stress growth caused by the change of elastic modulus E is more
 463 significant than that caused by the change of shape parameter m . In the part of peak stress, with
 464 the increase of parameter value, the peak strain decreases and the peak deviator stress increases;
 465 the change of elastic modulus E has more significant effect on the peak strain, while the shape
 466 parameter m has more obvious effect on the peak deviator stress. In the stress decreasing stage,
 467 the smaller the parameter value is, the slower the decreasing speed is, and the calculation curve is
 468 more sensitive to the change of elastic modulus E in this stage.

469 From the above diagram and analysis, it can be seen that the other four parameters except
 470 Poisson's ratio ν have a certain impact on the reconstruction curve. Under the condition of the
 471 same amplitude change, the influence of scale parameter a is the most obvious. Further
 472 comparative analysis: when multiple parameters change at the same time, the difference between

473 the reconstruction curve and the reference curve will not be discussed because Poisson's ratio ν
 474 has little influence on the reconstruction curve. The final result is shown in Figure 9.



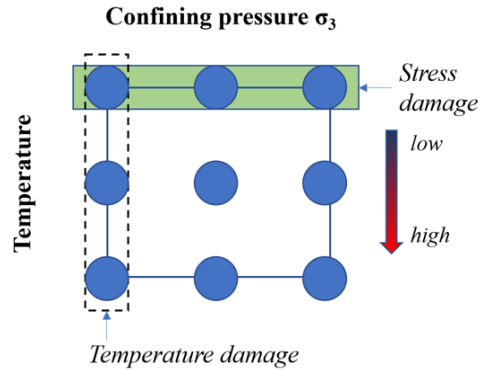
475

476 **Figure9.** Comparison of the influence of 10% increase or decrease of multi parameters of
 477 the model on the calculation curve

478 It is not difficult to find out from Figure. 9 that when multiple parameters change at the
 479 same time, the influence of each parameter will have a composite superposition effect, and the
 480 three stages of reconstruction stress-strain curve deviate greatly from the original datum curve.
 481 The variation of peak deviator stress is mainly due to the error of scale parameter a , and the
 482 deviation of stress growth stage is mainly due to the change of elastic modulus E and shape
 483 parameter m . The more fitting parameters are, the greater the influence of model parameter error
 484 on reconstruction curve accuracy is.

485 It can be seen from Table 4 that when the change of confining pressure and temperature
 486 is small, the change range of shape parameter m and scale parameter a is not large, but the final
 487 result is very sensitive to the change of these two parameters^[18]. When the binary polynomial
 488 fitting is used, the error of parameter simulation value will be further enlarged compared with
 489 that of single variable polynomial fitting. When the two parameters have errors at the same time,
 490 the uncertainty of the model will rise sharply, resulting in the reliability of the final result.

491 To sum up, it is necessary to predict the elastic modulus E , shape parameter m , scale
 492 parameter a , Poisson's ratio ν and friction angle φ under a certain target temperature and
 493 confining pressure state (non parametric experimental state) when the stress-strain curve of warm
 494 frozen soil is simulated simply by using the stress damage model. Among them, the elastic
 495 modulus E , shape parameter m and scale parameter a are affected by temperature and confining
 496 pressure changes at the same time, so binary function is needed to fit them. When using the
 497 coupled stress temperature damage model, only the shape parameter m , scale parameter a ,
 498 Poisson's ratio ν and the elastic modulus E at the target temperature are estimated. And different
 499 from the single stress damage model, the parameters needed in the stress-temperature coupled
 500 damage model can be fitted by only one element polynomial, which greatly reduces the
 501 uncertainty of parameter prediction.



502

503

Figure 10. Schematic diagram of experimental conditions of model parameters

504

505

506

507

508

509

510

511

512

Further compare the minimum experimental amount of the two parameter experiments. As shown in Figure. 10, in a certain temperature and confining pressure condition area, in order to predict any point, a single stress damage model needs at least 9 groups of experimental data to fit the parameters. However, if the stress-temperature coupled damage model is used, the temperature damage factor can be determined only by the experimental data of three groups of different confining pressures under the lowest temperature in the condition area, and the experimental data of three groups of different temperatures under any one of the three confining pressures, and the temperature damage factor can be determined, and the total minimum required is five groups of experimental data.

513

514

515

It can be seen that the stress-temperature coupled damage model is superior to the single stress-strain damage model in terms of the prediction accuracy of the stress-strain curve corresponding to the model and the experimental parameters.

516

517

6 Conclusion

518

519

520

521

522

Based on Hooke's law and strain equivalent theory of damage mechanics, the damage model of warm frozen soil structure under the coupling action of three-dimensional stress and temperature (stress-temperature coupled damage model) is established by using Weibull distribution to describe the damage of warm frozen soil element. Through theoretical analysis, mathematical derivation and experimental verification, the following conclusions are obtained:

523

524

525

526

527

(1) The composite damage theory is introduced into the stress-temperature coupled damage model of warm frozen soil. Based on Mohr-Coulomb criterion, the nominal stress is used to represent the stress damage of permafrost element, the initial elastic modulus is used to represent the temperature damage, and the composite damage factor is introduced to describe the coupling relationship between them, which makes the model more meaningful in theory.

528

529

530

531

532

533

(2) There are two general methods to solve the shape parameter m and scale parameter a of the stress temperature coupled damage model. Experimental results show that: for strain softening materials, when the confining pressure level is low, the difference between the two methods is small. However, under high confining pressure, the reconstruction curve obtained by the semi theoretical semi fitting method based on the characteristic points of the stress-strain curve is closer to the experimental curve.

534 (3) The results of triaxial compression experiments with constant temperature confining
535 pressure show that the stress-temperature coupled damage model has good simulation and
536 prediction ability. In the stage of stress development, the overall prediction accuracy of the
537 model is high; in the stage of stress peak, the prediction accuracy of the model decreases slightly
538 with the increase of confining pressure; in the same confining pressure, the prediction accuracy
539 of the model increases with the increase of the temperature of frozen soil.

540 (4) Compared with the single stress damage model, the stress-temperature coupled
541 damage model needs less model parameters, and only needs the one-dimensional function fitting
542 to complete the prediction. It can effectively reduce the influence of the system error caused by
543 the parameter estimation on the final results, effectively reduce the workload of the parameter
544 experiment, and improve the stability of the model.

545

546 **Acknowledgments**

547 Data used in this study is new data for the first time created for this research. We thank for National Natural Science
548 Foundation of China (41641024) for providing financial support.

549 **References**

- 550 Cao, W., & Zhang, S. (2005). Study on the statistical analysis of rock damage based on Mohr-
551 Coulomb criterion. *Journal of Hunan University*, 32(1), 43-47.
- 552 Dumais, S., & Konrad, J. M. (2017). One-dimensional large-strain thaw consolidation using
553 nonlinear effective stress–void ratio–hydraulic conductivity relationships. *Canadian*
554 *Geotechnical Journal*, 55(3), 414-426. doi:<https://doi.org/10.1139/cgj-2017-0221>
- 555 Esmaeili-Falak, M., Katebi, H., Javadi, A., & Rahimi, S. (2017). Experimental investigation of
556 stress and strain characteristics of frozen sandy soils-A case study of Tabriz subway.
557 *Modares Civil Engineering journal*, 17(5), 13-23.
- 558 Jia, H., Zi, F., Yang, G., Li, G., Shen, Y., Sun, Q., & Yang, P. (2019). Influence of Pore Water
559 (Ice) Content on the Strength and Deformability of Frozen Argillaceous Siltstone. *Rock*
560 *Mechanics Rock Engineering*, 1-8.
- 561 Jin, X., Yang, W., Meng, X., & Lei, L. (2019). Deduction and application of unfrozen water
562 content in soil based on electrical double-layer theory. *Rock and Soil Mechanics*, 40(04),
563 1449-1456.
- 564 Lai, Y., Jin, L., & Chang, X. (2009). Yield criterion and elasto-plastic damage constitutive model
565 for frozen sandy soil. *International Journal of Plasticity*, 25(6), 1177-1205.
- 566 Lai, Y., Li, S., Qi, J., Gao, Z., & Chang, X. (2008). Strength distributions of warm frozen clay
567 and its stochastic damage constitutive model. *Cold Regions Science Technology*, 53(2),
568 200-215. doi:<https://doi.org/10.1016/j.coldregions.2007.11.001>
- 569 Lemaitre, J. (2012). *A course on damage mechanics*, Springer Science & Business Media.
- 570 Li, G. (2009). Some problems in researches on constitutive model of soil. *Chinese Journal of*
571 *Geotechnical Engineering*, 10.

- 572 Li, S., Lai, Y., Zhang, M., & Zhang, S. (2007). Study on distribution laws of elastic modulus and
573 strength of warm frozen soil. *Chinese Journal of Rock Mechanics Engineering*, 26, 4299-
574 4305.
- 575 Li, S., Lai, Y., Zhang, S., & Liu, D. (2009). An improved statistical damage constitutive model
576 for warm frozen clay based on Mohr–Coulomb criterion. *Cold Regions Science and
577 Technology*, 57(2), 154-159. doi:<https://doi.org/10.1016/j.coldregions.2009.02.010>
- 578 Liu, S., & Zhang, J. (2012). Review on physic-mechanical properties of warm frozen soil.
579 *Journal of Glaciology Geocryology*, 34(1), 120-129.
- 580 Liu, Z., & Yu, X. (2011). Coupled thermo-hydro-mechanical model for porous materials under
581 frost action: theory and implementation. *Acta Geotechnica*, 6(2), 51-65.
582 doi:<https://xs.scihub.ltd/https://doi.org/10.1007/s11440-011-0135-6>
- 583 Ma, W., Wu, Z., Zhang, L., & Chang, X. (1999). Analyses of process on the strength decrease in
584 frozen soils under high confining pressures. *Cold Regions Science Technology*, 29(1), 1-
585 7. doi:[https://doi.org/10.1016/S0165-232X\(98\)00020-2](https://doi.org/10.1016/S0165-232X(98)00020-2)
- 586 Na, S., & Sun, W. (2017). Computational thermo-hydro-mechanics for multiphase freezing and
587 thawing porous media in the finite deformation range. *Computer Methods in Applied
588 Mechanics Engineering*, 318, 667-700. doi:<https://doi.org/10.1016/j.cma.2017.01.028>
- 589 Nassr, A., Esmaeili-Falak, M., Katebi, H., & Javadi, A. (2018). A new approach to modeling the
590 behavior of frozen soils. *Engineering geology*, 246, 82-90.
591 doi:<https://doi.org/10.1016/j.enggeo.2018.09.018>
- 592 Ning, J., & Zhu, Z. (2007). Constitutive model of frozen soil with damage and numerical
593 simulation of the coupled problem. *Chinese Journal of Theoretical Applied Mechanics*, 1.
- 594 Qi, J., & MA, W. (2010). State-of-art of research on mechanical properties of frozen soils. *Rock
595 Soil Mechanics*, 31(1), 133-143.
- 596 Song, B., Liu, E., & Zhang, D. (2019). Experimental study on the mechanical properties of warm
597 frozen silt soils. *Journal of Glaciology and Geocryology*, 41(03), 595-605.
- 598 Wei, Z., Jin, H., Zhang, J., Yu, S., Han, X., Ji, Y., He, R., & Chang, X. (2011). Prediction of
599 permafrost changes in Northeastern China under a changing climate. *Science China Earth
600 Sciences*, 54(6), 924-935.
- 601 Xu, W., & Wei, L. (2002). Study on statistical damage constitutive model of rock. *Chinese
602 Journal of Rock Mechanics Engineering*, 21(6), 787-791.
- 603 Xu, X., Li, Q., Lai, Y., Pang, W., & Zhang, R. (2019). Effect of moisture content on mechanical
604 and damage behavior of frozen loess under triaxial condition along with different
605 confining pressures. *Cold Regions Science Technology*, 157, 110-118.
606 doi:<https://doi.org/10.1016/j.coldregions.2018.10.004>
- 607 Xu, X., Wang, J., & Zhang, L. (2001). *Frozen soil physics*. Beijing, Beijing Science Technology
608 Press, .
- 609 Xu, X., Wang, Y., Bai, R., Zhang, H., & Hu, K. (2016). Effects of sodium sulfate content on
610 mechanical behavior of frozen silty sand considering concentration of saline solution.
611 *Results in physics*, 6, 1000-1007. doi:<https://doi.org/10.1016/j.rinp.2016.11.040>

- 612 Yan, C., Wang, T., Jia, H., Xu, W., & Zi, F. (2019). Influence of the unfrozen water content on
613 the shear strength of unsaturated silt during freezing and thawing. *Chinese Journal of*
614 *Rock Mechanics and Engineering*, 38(06), 1252-1260.
- 615 Yu, S., Deng, H., & Zhang, Y. (2018). The constitutive relationship of rock damage considering
616 the effect of temperature and confining pressure. *Journal of Railway Science*
617 *Engineering*, 15, 1-9.
- 618 Zhang, D., Liu, E., Liu, X., Zhang, G., Yin, X., & Song, B. (2018). A damage constitutive model
619 for frozen sandy soils based on modified Mohr-Coulomb yield criterion. *Chinese Journal*
620 *of Rock Mechanics Engineering*, 37(4), 978-986.
- 621 Zhang, H., & Yang, G. (2010). Research on damage model of rock under coupling action of
622 freeze-thaw and load. *Chinese Journal of Rock Mechanics Engineering*, 29(3), 471-476.
- 623 Zhang, M., Pei, W., Li, S., Lu, J., & Jin, L. (2017). Experimental and numerical analyses of the
624 thermo-mechanical stability of an embankment with shady and sunny slopes in a
625 permafrost region. *Applied Thermal Engineering*, 127, 1478-1487.
626 doi:<https://doi.org/10.1016/j.applthermaleng.2017.08.074>
- 627 Zhang, Y., & Michalowski, R. L. (2015). Thermal-hydro-mechanical analysis of frost heave and
628 thaw settlement. *Journal of geotechnical geoenvironmental engineering*, 141(7),
629 04015027. doi:[https://doi.org/10.1061/\(ASCE\)GT.1943-5606.0001305](https://doi.org/10.1061/(ASCE)GT.1943-5606.0001305)
- 630 Zhou, Y., Guo, D., Qiu, G., Cheng, G., & Li, S. (2000). *Geocryology in China*. Beijing, Chinese
631 Academy of Sciences.
632